

Kennesaw State University
DigitalCommons@Kennesaw State University

Faculty Publications

10-2015

Performance Limiting Factors of $\text{Cu}_2\text{ZnSn}(\text{S}_x\text{Se}_{1-x})_4$ Solar Cells Prepared by Thermal Evaporation

Sandip Das

Kennesaw State University, sdas2@kennesaw.edu


Raghu N. Bhattacharya

National Renewable Energy Laboratory

Krishna C. Mandal

Kennesaw State University

Follow this and additional works at: <https://digitalcommons.kennesaw.edu/facpubs>

 Part of the [Bioresource and Agricultural Engineering Commons](#), and the [Power and Energy Commons](#)

Recommended Citation

Das, Sandip; Bhattacharya, Raghu N.; and Mandal, Krishna C., "Performance Limiting Factors of $\text{Cu}_2\text{ZnSn}(\text{S}_x\text{Se}_{1-x})_4$ Solar Cells Prepared by Thermal Evaporation" (2015). *Faculty Publications*. 4168.

<https://digitalcommons.kennesaw.edu/facpubs/4168>

This Article is brought to you for free and open access by DigitalCommons@Kennesaw State University. It has been accepted for inclusion in Faculty Publications by an authorized administrator of DigitalCommons@Kennesaw State University. For more information, please contact digitalcommons@kennesaw.edu.

Performance limiting factors of $\text{Cu}_2\text{ZnSn}(\text{S}_x\text{Se}_{1-x})_4$ solar cells prepared by thermal evaporation

Sandip Das^{1‡}, Raghu N. Bhattacharya², and Krishna C. Mandal^{1*}

¹Department of Electrical Engineering, University of South Carolina, Columbia, SC 29208, USA

²National Renewable Energy Laboratory, 1617 Cole Boulevard, Golden, CO 80401, USA

[‡]Present address: Department of Electrical Engineering, Kennesaw State University, Marietta, GA 30060, USA

*Corresponding author: Tel.: +1 803 777 2722; fax: +1 803 777 8045. E-mail address: mandalk@cec.sc.edu (K.C. Mandal).

Abstract

$\text{Cu}_2\text{ZnSn}(\text{S}_x\text{Se}_{1-x})_4$ (CZTSSe) thin film solar cells have been prepared by vacuum-based thermal evaporation of metal and binary sulfide precursors followed by annealing in a mixed chalcogen vapor at 550°C for one hour. The Zn/Sn ratio in the precursor was varied from 0.75-1.50 keeping the Cu/(Zn+Sn) ratio constant at 0.7. The best performing solar cell was obtained with a final film composition of Cu/(Zn+Sn) = 0.77 and Zn/Sn = 1.13 corresponding to a Zn/Sn ratio of 0.9 in the precursor. The champion cell exhibited an open-circuit voltage (V_{OC}) of 506 mV, short-circuit current density (J_{SC}) of 22.92 mA/cm², and a fill factor (FF) of 35% resulting in a total area efficiency (η) of 4.06% without any antireflection coating. Cell performance was found to be limited by high series resistance (R_s) = 31.1 Ω and a low shunt resistance (R_{sh}) = 125.2 Ω . No detrimental secondary phases, such as $\text{Cu}_{2-x}\text{S}(\text{Se})$ or ZnS were detected in the absorber film. Microstructural investigation suggested that small multigrain structure of the CZTSSe absorber layer, presence of an interfacial $\text{Mo}(\text{S},\text{Se})_y$ blocking barrier, and micro air-voids at the Mo back contact are the major contributors to the origin of high R_s . Morphological study of the CZTSSe film surface by atomic force microscopy revealed micro-pores that act as low resistance shunt paths and explains the source of such low R_{sh} . The performance limiting factors of the vacuum based thermally evaporated CZTSSe thin film solar cells are reported.

Keywords: CZTSSe, Thin film, Solar cell, Thermal evaporation, Earth-abundant

1. Introduction

Cu-based kesterite compound, $\text{Cu}_2\text{ZnSn}(\text{S}_x\text{Se}_{1-x})_4$ (CZTSSe) has recently emerged as the most promising photo-absorber material for low-cost high-efficiency thin film solar cells (TFSC), alternative to the current benchmark TFSC technologies based on CuInGaSe_2 (CIGS) and CdTe absorbers [1-5]. A tunable direct bandgap in the range of 1.0-1.5 eV for optimal terrestrial photoconversion and a large optical absorption coefficient in the order of 10^4 - 10^5 cm^{-1} makes CZTSSe an excellent solar absorber for thin film solar cells. Using earth-abundant, non-toxic, and relatively inexpensive constituent elements, CZTSSe can support terawatt-scale module production in the near future and resolves commercial sustainability and/or environmental issues pertaining to CIGS/CdTe-based technologies [6, 7].

Efficiency of the CZTSSe-based thin film solar cells have been improved quite significantly over the past decade since the first report by Katagiri et al. in 1997 [1]. Several fabrication routes for the absorber layer preparation have been investigated including vacuum-based evaporation [1-5] and sputtering techniques [8, 9], as well as non-vacuum approaches using nanoparticle inks [10, 11], hydrazine-based solution-particle slurry [12, 13], electrodeposition [14, 15], spray pyrolysis [16, 17], and open atmosphere chemical vapor deposition (OACVD) [18]. Recently, an astounding photoconversion efficiency of 12.6% has been reported for CZTSSe solar cells with the absorber layer prepared by a non-vacuum process developed by IBM group that used hydrazine-based hybrid solution-particle slurry [13]. However, use of highly toxic and hazardous hydrazine severely limits the scalability of this process for commercial production.

On the other hand, vacuum-based physical vapor deposition methods are well-established standards for growing high-quality thin films in the semiconductor industry. Particularly, thermal evaporation method has been proved to be a commercially scalable and cost effective method to grow high quality CIGS and CdTe thin films in the past with unprecedented reproducibility, achieving high efficiency solar cells [19, 20]. In this article, we report on the fabrication and characterization of CZTSSe solar cells prepared by vacuum-based thermal evaporation

technique. The investigation results specifically focused on the identification of the major factors that play key role in the photovoltaic performance of the thermally evaporated CZTSSe solar cells and directly correlate their electronic/photovoltaic properties with the absorber layer composition, microstructure, and back contact interface. Our results suggest the possible pathways for further improvements of the kesterite CZTSSe-based solar cells.

2. Experimental

2.1. CZTSSe absorber film and solar cell fabrication

The CZTSSe photoactive absorber layer was prepared in a vacuum-based two-step process. In the first step, high purity ZnS (99.99%), Cu (99.999%), and Sn (99.999%) were evaporated sequentially on molybdenum (Mo) coated soda-lime glass (SLG) substrates forming a stacked precursor layer of ZnS/Cu/Sn on SLG/Mo. In the second step, the precursor stacks were annealed under a mixed sulfur and selenium vapor at 550°C for one hour under atmospheric pressure to react with the precursor stack forming the polycrystalline CZTSSe film. The bi-layer Mo back contact with an approximate thickness of 700 nm was deposited by DC sputtering on the SLG substrate. A vacuum thermal evaporator (CHA - SE 600) was used for the physical vapor deposition of ZnS, Cu, and Sn precursors. The thermal evaporation system is equipped with three individual sources and all three layers of the precursor stacks were sequentially deposited in one vacuum cycle. A base vacuum of 2×10^{-6} torr was attained prior to the deposition. An Inficon XTC/2 thin film deposition controller connected to a quartz crystal thickness monitor was programmed for automated deposition of each layer in the stack within $\pm 1\%$ tolerance of the desired value.

Photovoltaic (PV) performance of CZTSSe-based solar cell is highly composition sensitive [21]. The major challenge in fabricating a PV grade CZTSSe absorber layer is to control the final film composition that is favorable for an efficient solar cell. As a general consensus, high efficiency cells could be obtained with a Cu-poor and Zn-rich composition in the absorber layer, whereas

stoichiometric films have been reported to show inferior PV performance. During the high temperature sulfurization/selenization process, Sn loss from the precursor as volatile $\text{Sn}(\text{S},\text{Se})_2$ have been reported, which complicates the film growth process. Also, the processing parameters during the absorber growth, such as peak temperature, temperature profile, annealing duration, S/Se vapor pressure etc. play key role in the quality of the fabricated films and resulting photovoltaic properties. Therefore, fabrication of a good quality CZTSSe absorber film is a challenging task. We have fabricated 7 sets of precursor films with a composition variation in a broad range. The Zn/Sn ratio was varied from 0.75-1.50 keeping the Cu/(Zn+Sn) ratio fixed at 0.7. The composition variation was achieved by changing relative thickness of the precursor layers in the stack. ZnS thickness was kept constant at 300 nm for all precursors while the thickness of Cu and Sn layers were varied to obtain different compositions of the precursors. The details of all precursor layer thicknesses and compositions are summarized in Table I. The heterojunction was formed by a thin (~50 nm) n-CdS layer deposited on the as-grown p-CZTSSe films by a low-cost chemical bath deposition (CBD) technique. Rest of the device was completed following the structure of a standard CIGS cell with a final device structure of SLG/Mo/p-CZTSSe/n-CdS/i-ZnO/Al:ZnO/Al. Individual cells were mechanically scribed after completion of the entire device fabrication process. Measured individual cell areas were approximately 0.42 cm² with about 5% shading incurred due to the top Al grid lines. No antireflection coating was deposited on the devices reported here.

2.2. CZTSSe film and solar cell characterization

Elemental atomic composition and phase purity of the as-grown CZTSSe films were investigated by energy dispersive X-ray spectroscopy (EDX) and Raman spectroscopy respectively. The film surface morphology was studied by atomic force microscopy (AFM). Out of seven precursor sets as detailed in Table I, the cells fabricated on the CZTSSe film

corresponding to the precursor set 3c showed best photovoltaic performance with the champion cell efficiency of 4.06%.

Raman spectroscopy was performed using a micro-Raman setup equipped with a 632 nm laser of $\sim 2 \mu\text{m}$ spot size. The setup was calibrated to known Si peak at 520.7 cm^{-1} prior to the measurement. SEM images and EDX data were collected using a high resolution Zeiss Ultraplus field emission scanning electron microscope (FESEM) equipped with EDX microanalysis. It is to note that the EDX data were collected on the bare CZTSSe film surface without the top CdS/ZnO layers for best accuracy. AFM imaging was carried out using a Picoplus AFM setup operated in tapping mode.

J-V characteristics of the solar cells were measured using a Keithley 237 source-measure unit (SMU) and data acquisition was performed through custom-built Labview program. The PV performance of the cells were measured under calibrated AM 1.5 (100 mW/cm^2) simulated solar irradiation using an Oriel (Newport corporation) class ABB solar simulator. The maximum increase of the cell temperature during the measurement under illumination was limited to $<2^\circ\text{C}$.

3. Results and discussion

3.1. CZTSSe film properties

Structural and compositional studies of the CZTSSe films were carried out by Raman spectroscopy and EDX analysis. Raman spectra of the CZTSSe absorber film corresponding to each cell (1-7) are plotted in Fig. 1 (a). Peak positions of possible binary and ternary phases (marked with black arrows) along with the signature peak positions for pentanary kesterite CZTSSe (marked with red arrows) are shown in Fig 1(b) as reference. The major peak corresponding to 326.6 cm^{-1} is attributed to the A1 vibrational mode of the sulfur atoms present in the CZTSSe crystal lattice. The other broad peak at lower wavenumber region consists of two individual peaks – one at 211.5 cm^{-1} and the other at 218.1 cm^{-1} . The peak at 211.5 cm^{-1} is attributed to the A1 vibrational mode of Se atoms in CZTSSe and is in well agreement with the

reported Raman shifts observed in CZTSSe thin films and bulk crystals [22-26]. The other peak at 218.1 cm^{-1} corresponds to a SnS secondary phase which formed during sulfurization/selenization process. Also, the small peak detected at 191.8 cm^{-1} can be attributed to the SnS/SnSe₂ phases. Two other relatively less intense Raman peaks related to CZTSSe were found at 176.4 cm^{-1} and 229 cm^{-1} as indexed in Fig 1(a). However, no other eminent peaks corresponding to secondary phases, such as ZnSe (205 cm^{-1} and 251 cm^{-1}), Cu_{2-x}S/Cu_{2-x}Se ($475\text{ cm}^{-1}/260\text{ cm}^{-1}$), Sn₂S₃ (304 cm^{-1}), and Cu₂SnS₃/Cu₂SnSe₃ ($318\text{ cm}^{-1}/180\text{ cm}^{-1}$) were observed for Cell 2-7. Cell 1 showed formation of Cu₂SnS₃/Cu₂SnSe₃ phases along with SnSe₂ and a trace of ZnS other than the Sn-chalcogenide phases. Hsu et al. reported that the ternary copper-tin-sulfide/selenide phase forms during the sulfurization/selenization process which further reacts with the binary ZnS resulting in the quaternary CZTS/CZTSe [27]. Presence of undesired binary/ternary phases in the absorber film suggests incomplete sulfurization/selenization or incomplete phase transformation. These secondary phases are expected to adversely affect the cell performance which is evident from the PV performance measurements on Cell 1. A prominent peak corresponding to CZTS appeared in Cell 2 and the Cu₂SnSe₃ phase disappeared. However, SnS/SnSe₂ phases and a trace amount of ZnS could still be observed. The broad peaks corresponding to Cell 3 suggests existence of the undesired Sn-chalcogenide binary phases as evident from the small humps. The Raman data indicates that Cell 4-7 were sufficiently sulfurized/selenized with sharp peaks corresponding to CZTSSe and without any significant secondary peaks other than SnS which supports the superior photovoltaic response of Cell 4. The possible reason for incomplete reaction at Cell 1 location is the obstruction of smooth lateral flow of S/Se vapor by the edge of the horizontally placed substrate.

The elemental composition analysis data for the film corresponding to cell 4 are summarized in Table II. Composition of the CZTSSe film was found to be Cu-poor and slightly Zn-rich with a Cu/(Zn+Sn) ratio of 0.773 and a Zn/Sn ratio of 1.13. It is evident that considerable amount of Sn

was lost in the sulfurization/selenization stage which turned the Sn-rich precursor into a Zn-rich film.

3.2. Photovoltaic performance and device characteristics

The J-V characteristics of cell 4 under dark and under AM 1.5 (100 mW/cm²) illumination are shown in Fig. 2. The champion cell (cell 4) exhibited an open-circuit voltage (V_{OC}) of 506 mV, short-circuit current density (J_{SC}) of 22.92 mA/cm², and a fill factor (FF) of 35% resulting in a total area efficiency of 4.06%. A series resistance (R_s) of 31.1 Ω and a shunt resistance (R_{sh}) of 125.2 Ω were calculated from the illuminated J-V data. Dark and illuminated J-V crossover was observed at ~ 0.55 V which signifies the presence of a large series resistance. The cell performance is clearly limited by the high R_s , low R_{sh} , and a poor fill factor. A further analysis of the device microstructure provides insight into the origin of such high R_s and low R_{sh} as discussed in section 3.3. Measured photovoltaic performance parameters of all other cells on the same substrate (3c) are summarized in Table III.

The dark J-V characteristic of the thin film heterojunction solar cell was fitted according to equation (1) considering a two-diode model and are plotted in a semi-log graph in Fig. 3 showing each component.

$$J = J_{01} \left[\exp\left(\frac{V - JR_s}{n_1 kT}\right) - 1 \right] + J_{02} \left[\exp\left(\frac{V - JR_s}{n_2 kT}\right) - 1 \right] + \frac{V - JR_s}{R_{sh}} \quad (1)$$

Where, J_{01} , J_{02} are the reverse saturation current densities and n_1 , n_2 are the ideality factors of diode 1 and diode 2 respectively. V is the applied voltage, T is temperature in Kelvin, k is the Boltzmann constant, R_s and R_{sh} are the series and shunt resistances respectively. A value of $J_{01} = 1.8 \times 10^{-5}$ A/cm², $n_1 = 3.9$ and $J_{02} = 5.1 \times 10^{-9}$ A/cm², $n_2 = 2.15$ were extracted from the experimental data fitting.

3.3. Microstructural analysis

The compositional analysis did not indicate the formation of any detrimental secondary phases, such as $\text{Cu}_{2-x}\text{S}(\text{Se})$ and $\text{ZnS}(\text{Se})$ which are known contributors for reduced shunt-resistance and high series resistance respectively in CZTSSe-based devices. Therefore, we studied the device microstructure to investigate the origin of such high R_s and low R_{sh} in our cells.

The film surface morphology was investigated by AFM and is shown in Fig. 4. The average and rms roughness of the surface were calculated using the following formula:

$$R_{avg} = \frac{1}{N} \int_0^L |Z(x)| dx \approx \frac{1}{N} \sum_{n=1}^N |Z_n - \bar{Z}| \quad (2)$$

$$R_{rms} = \sqrt{\frac{1}{N} \int_0^L |Z^2(x)| dx} \approx \sqrt{\frac{1}{N} \sum_{n=1}^N (Z_n - \bar{Z})^2} \quad (3)$$

where N is the total number of points within the region of analysis, L is the evaluation length over which the analysis is performed, $Z(x)$ is the function defining the measured surface profile, \bar{Z} is the mean surface height relative to the center plane within the analysis area, and Z_n is the height of point n in the z -direction. The average and rms roughness of the film were calculated to be 70.8 nm and 88.4 nm respectively. An important morphological feature observed was the presence of micro-pores as marked by arrows in the figure. These micro-pores essentially act as the low resistance shunt paths and are attributed to the primary reason for low R_{sh} . Existence of such pores on CZTSSe films have been reported by other researchers [28-29]. In our solar cells, the micropores have formed during the sulfo-selenization process and can be attributed to the change of volume during the solid state reactions or during ramp down. Optimization of the film composition and microstructure is the key to further improve the cell efficiencies which can be achieved by optimization of the film growth parameters (such as temperature profile, S/Se vapor pressure etc.) during annealing of the precursor stacks. Also, post-growth annealing of the film may aid stress relief and healing of the pores.

The cross-sectional SEM image of the completed solar cell showing the microstructure of the device is presented in Fig. 5. A number of notable features were observed from the SEM image. The CZTSSe layer showed small multiple grains in the z-direction with different grain sizes ranging from ~0.3-0.8 μm . Such smaller multigrain structure presents grain boundaries in the transverse direction to the transport path of the photogenerated carriers across the cell which acts as recombination center and hinders carrier transport. These phenomena are well known for limiting the photogenerated current and reduce fill factor in polycrystalline thin film solar cells. The second notable observation was the presence of micro air-voids at the back contact. This reduces the effective contact area leading to an increased series resistance. We believed that further optimization of the film growth parameters will lead to the elimination of these undesired air-voids. The third observation is clearly the formation of a thin (~150 nm) $\text{Mo}(\text{S},\text{Se})_y$ interfacial layer between the CZTSSe film and the Mo back contact seen as a darker contrast region. It is reported that such interfacial layer behave as a blocking barrier and affects charge transport. Control of the thickness of this $\text{Mo}(\text{S},\text{Se})_y$ interfacial layer is important and can be achieved by further optimization of process parameters during sulfo-selenization. The above observations explain the origin of high R_s and low FF exhibited by our fabricated solar cells. Many of the CZTSSe cells with comparable efficiencies reported in the literature suffer from significant amounts of detrimental $\text{Cu}_{2-x}\text{S}(\text{Se})$, $\text{Cu}_2\text{SnS}(\text{Se})_3$, and/or $\text{SnS}(\text{Se})_2$ compound formation [30-32]. These highly conductive secondary phases are far more detrimental to the device performance as it creates shunt paths throughout the device leading to a low R_{sh} . In our fabricated array, the superior cells (such as Cell 4) were free from these device killing secondary phases. We believe that optimization of the film growth parameters will help achieve a more uniform large-area array with higher cell efficiencies.

4. Conclusions

In this work, we have successfully fabricated monolithic arrays of CZTSSe solar cells using a vacuum-based evaporation technique. Structural, compositional, and morphological properties of the CZTSSe films were investigated by Raman spectroscopy, EDX, and AFM respectively. Photovoltaic performance and the diode characteristics of the cells were measured under AM 1.5 illumination and under dark. Compositional analysis showed a slightly Zn-rich and Cu-poor stoichiometry and existence of SnS(Se)/SnS(Se)₂ secondary phases. PV performance of kesterite-based solar cells are highly sensitive to its composition and microstructure. The high series resistance and poor fill factor were attributed to the presence of small multigrain structure of the absorber layer, micro air-voids, and a Mo(S,Se)_y blocking barrier at the Mo back contact interface. The low shunt resistance is attributed to the micro-pores observed in the CZTSSe acting as low resistance shunt paths. We conclude that improvement of the microstructure by optimization of the fabrication process parameters is the most important aspect to enhance efficiency of these solar cells. Further investigations on quantitative analysis of the recombination loss in these devices are presently underway.

Acknowledgements

The authors (S. Das and K.C. Mandal) acknowledge partial financial support provided by DARPA (grant # N66001-10-1-4031) for this investigation. One of the authors (R.N. Bhattacharya, NREL) would like to acknowledge partial financial support from 'Alliance for Sustainable Energy, LLC', under contract number DE-AC36-08GO28308 with the U.S. Department of Energy (LDRD program).

References:

- [1] H. Katagiri, N. Sasaguchi, S. Hando, S. Hoshino, J. Ohashi, T. Yokota, Preparation and evaluation of $\text{Cu}_2\text{ZnSnS}_4$ thin films by sulfurization of E-B evaporated precursors, *Sol. Energy Mater. Sol. Cells* 49 (1997) 407-414.
- [2] B.-A. Schubert, B. Marsen, S. Cinque, T. Unold, R. Klenk, S. Schorr, H.-W. Schock, $\text{Cu}_2\text{ZnSnS}_4$ thin film solar cells by fast coevaporation, *Prog. Photovolt. Res. Appl.* 19 (2011) 93-96.
- [3] I. Repins, C. Beall, N. Vora, C. DeHart, D. Kuciauskas, P. Dippo, B. To, J. Mann, W.-C. Hsu, A. Goodrich, R. Noufi, Co-evaporated $\text{Cu}_2\text{ZnSnSe}_4$ films and devices, *Sol. Energy Mater. Sol. Cells* 101 (2012) 154-159.
- [4] K. Wang, O. Gunawan, T. Todorov, B. Shin, S.J. Chey, N.A. Bojarczuk, D. Mitzi, S. Guha, Thermally evaporated $\text{Cu}_2\text{ZnSnS}_4$ solar cells, *Appl. Phys. Lett.* 97 (2010) 143508.
- [5] S. Das, K.C. Mandal, Comparison of $\text{Cu}_2\text{ZnSnS}_4$ thin-film properties prepared by thermal evaporation of elemental metals and binary sulfide sources, *Photovoltaic Specialists Conference (PVSC), 38th IEEE, 2012*, pp. 2674-2678.
- [6] M.A. Green, Estimates of Te and In prices from direct mining of known ores, *Prog. Photovolt. Res. Appl.* 17 (2009) 347-359.
- [7] V.M. Fthenakis, P.D. Moskowitz, Thin-film photovoltaic cells: health and environmental issues in their manufacture use and disposal, *Prog. Photovolt. Res. Appl.* 3 (1995) 295-306.
- [8] H. Katagiri, K. Jimbo, S. Yamada, T. Kamimura, W.S. Maw, T. Fukano, T. Ito, T. Motohiro, Enhanced conversion efficiencies of $\text{Cu}_2\text{ZnSnS}_4$ -based thin film solar cells by using preferential etching technique, *Appl. Phys. Express*, 1 (2008) 041201.
- [9] G. Zoppi, I. Forbes, R.W. Miles, P.J. Dale, J.J. Scragg, L.M. Peter, $\text{Cu}_2\text{ZnSnSe}_4$ thin film solar cells produced by selenisation of magnetron sputtered precursors, *Prog. Photovolt. Res. Appl.* 17 (2009) 315-319.

- [10] Q. Guo, G.M. Ford, W.-C. Yang, B.C. Walker, E.A. Stach, H.W. Hillhouse, R. Agrawal, Fabrication of 7.2% efficient CZTSSe solar cells using CZTS nanocrystals, *J. Am. Chem. Soc.* 132 (2010) 17384-17386.
- [11] Y. Cao, M.S. Denny Jr., J.V. Caspar, W.E. Farneth, Q. Guo, A.S. Ionkin, L.K. Johnson, M. Lu, I. Malajovich, D. Radu, H.D. Rosenfeld, K.R. Choudhury, W. Wu, High-efficiency solution-processed $\text{Cu}_2\text{ZnSn}(\text{S},\text{Se})_4$ thin-film solar cells prepared from binary and ternary nanoparticles, *J. Am. Chem. Soc.* 134 (2012) 15644-15647.
- [12] D.A.R. Barkhouse, O. Gunawan, T. Gokmen, T.K. Todorov, D.B. Mitzi, Device characteristics of a 10.1% hydrazine-processed $\text{Cu}_2\text{ZnSn}(\text{Se},\text{S})_4$ solar cell, *Prog. Photovolt. Res. Appl.* 20 (2012) 6-11.
- [13] W. Wang, M.T. Winkler, O. Gunawan, T. Gokmen, T.K. Todorov, Y. Zhu, D.B. Mitzi, Device characteristics of CZTSSe thin-film solar cells with 12.6% efficiency, *Adv. Energy Mater.* 4 (2014) 1301465.
- [14] S. Ahmed, K.B. Reuter, O. Gunawan, L. Guo, L.T. Romankiw, H. Deligianni, A high efficiency electrodeposited $\text{Cu}_2\text{ZnSnS}_4$ solar cell, *Adv. Energy Mater.* 2 (2012) 253-259.
- [15] R.N. Bhattacharya, 3.6%-CZTSSe device fabricated from ionic liquid electrodeposited Sn layer, *The Open Surf. Sci. Journal* 5 (2013) 21-24.
- [16] X. Zeng, K.F. Tai, T. Zhang, C.W. J. Ho, X. Chen, A. Huan, T.C. Sum, L.H. Wong, $\text{Cu}_2\text{ZnSn}(\text{S},\text{Se})_4$ kesterite solar cell with 5.1% efficiency using spray pyrolysis of aqueous precursor solution followed by selenization, *Sol. Energy Mater. Sol. Cells* 124 (2014) 55-60.
- [17] S. Das, C. Frye, P.G. Muzykov, K.C. Mandal, Deposition and characterization of low-cost spray pyrolyzed $\text{Cu}_2\text{ZnSnS}_4$ (CZTS) thin-films for large-area high-efficiency heterojunction solar cells, *ECS Trans.* 45 (2012) 153-161.
- [18] T. Washio, T. Shinji, S. Tajima, T. Fukano, T. Motohiro, K. Jimbo, H. Katagiri, 6% Efficiency $\text{Cu}_2\text{ZnSnS}_4$ -based thin film solar cells using oxide precursors by open atmosphere type CVD, *J. Mater. Chem.* 22 (2012) 4021-4024.

- [19] I. Repins, M.A. Contreras, B. Egaas, C. DeHart, J. Scharf, C.L. Perkins, B.To, R. Noufi, 19.9%-efficient ZnO/CdS/CuInGaSe₂ solar cell with 81.2% fill factor, *Prog. Photovolt. Res. Appl.* 16 (2008) 235-239.
- [20] M. Gloeckler, I. Sankin, Z. Zhao, CdTe solar cells at the threshold to 20% efficiency, *IEEE J. Photovoltaics*, 3 (2013) 1389-1393.
- [21] T.K. Todorov, K.B. Reuter, D.B. Mitzi, High-efficiency solar cell with earth-abundant liquid-processed absorber, *Adv. Mater.* 22 (2010) E156-E159.
- [22] M. Grossberg, J. Krustok, J. Raudoja, K. Timmo, M. Altosaar, T. Raadik, Photoluminescence and Raman study of Cu₂ZnSn(Se_xS_{1-x})₄ monograins for photovoltaic applications, *Thin Solid Films* 519 (2011) 7403-7406.
- [23] S. Das, R.M. Krishna, S. Ma, K.C. Mandal, Single phase polycrystalline Cu₂ZnSnS₄ grown by vertical gradient freeze technique, *J. Crystal Growth* 381 (2013) 148-152.
- [24] S. Das, K.C. Mandal, Cu₂ZnSnSe₄ photovoltaic absorber grown by vertical gradient freeze technique, *Jpn. J. Appl. Phys.* 52 (2013)125502-1-125502-4.
- [25] A.-J. Cheng, M. Manno, A. Khare, C. Leighton, S.A. Campbell, E.S. Aydil, Imaging and phase identification of Cu₂ZnSnS₄ thin films using confocal Raman spectroscopy, *J. Vac. Sci. Technol. A* 29 (2011) 051203-1- 051203-11.
- [26] S. Das, K.C. Mandal, Growth and characterization of kesterite Cu₂ZnSn(S_xSe_{1-x})₄ crystals for photovoltaic applications, *Mater. Res. Bull.* 57 (2014) 135-139.
- [27] W.-C. Hsu, B. Bob, W. Yang, C.-H. Chung, Y. Yang, Reaction pathways for the formation of Cu₂ZnSn(Se,S)₄ absorber materials from liquid-phase hydrazine-based precursor inks, *Energy Environ. Sci.* 5 (2012) 8564-8571.
- [28] K.V. Gurav, S.W. Shina, U.M. Patil, M.P. Suryawanshi, S.M. Pawar, M.G. Gang, S.A. Vanalakar, J.H. Yun, J.H. Kim, Improvement in the properties of CZTSSe thin films by selenizing single-step electrodeposited CZTS thin films, *J. Alloy. Compd.* 631 (2015) 178-182.

- [29] K. Woo, Y. Kim, W. Yang, K. Kim, I. Kim, Y. Oh, J.Y. Kim, J. Moon, Band-gap-graded $\text{Cu}_2\text{ZnSn}(\text{S}_{1-x}\text{Se}_x)_4$ Solar Cells Fabricated by an Ethanol-based, particulate precursor Ink Route, *Sci. Rep.* 3 (2013) 3069.
- [30] L.-C. Wang, Y.-C. Lin, Effect of the stacked structure on performance in CZTSSe thin film solar cells, *Appl. Surf. Sci.* (2015), <http://dx.doi.org/10.1016/j.apsusc.2015.05.104>
- [31] S. Temgoua, R. Bodeux, N. Naghavi, S. Delbos, Effects of SnSe_2 secondary phases on the efficiency of $\text{Cu}_2\text{ZnSn}(\text{S}_x\text{Se}_{1-x})_4$ based solar cells, *Thin Solid Films*, 582 (2015) 215-219.
- [32] G.Y. Kim, W. Jo, K.D. Lee, H.-S. Choi, J.Y. Kim, H.-Y. Shin, T.T.T. Nguyen, S. Yoon, B.S. Joo, M. Gu, M. Han, Optical and surface probe investigation of secondary phases in $\text{Cu}_2\text{ZnSnS}_4$ films grown by electrochemical deposition, *Sol. Energy Mater. Sol. Cells* 139 (2015) 10-18.

Table I. Summary of the precursor layer thickness and compositions for seven sets of precursor stacks.

Stack ID	Thickness of precursor stack layers (nm)				Precursor elemental ratios		
	<i>ZnS</i>	<i>Cu</i>	<i>Sn</i>	Total thickness	$\frac{Cu}{(Zn + Sn)}$	$\frac{Zn}{Sn}$	$\frac{Chalcogen}{Metals}$
2c	300	146	273	719	0.7	0.75	0.252
3c	300	132	227	659	0.7	0.90	0.279
8a	300	126	205	631	0.7	1.00	0.293
3b	300	120	186	606	0.7	1.10	0.308
5b	300	116	172	588	0.7	1.20	0.319
2d	300	111	158	569	0.7	1.30	0.332
4d	300	105	136	541	0.7	1.50	0.353

Table II. Summary of the precursor layer thickness and compositions for seven sets of precursor stacks.

Composition of CZTSSe film: Cell 4					Elemental ratios			
<i>Cu</i> (at%)	<i>Zn</i> (at%)	<i>Sn</i> (at%)	<i>S</i> (at%)	<i>Se</i> (at%)	$\frac{Cu}{(Zn + Sn)}$	$\frac{Zn}{Sn}$	$\frac{S}{(S + Se)}$	$\frac{Chalcogen}{Metals}$
15.49	10.64	9.41	37.56	26.91	0.773	1.13	0.583	1.815

Table III. Photovoltaic performance parameters of the fabricated solar cells calculated from the illuminated J-V characteristics at room temperature under AM1.5 irradiation.

Cell No.	V_{oc} (mV)	J_{sc} (mA/cm ²)	FF (%)	R_s (Ω)	R_{sh} (Ω)	P_{max} (mW)	η (%)
1	483	17.94	33.5	37.0	113.1	1.217	2.90
2	484	19.38	32.8	36.9	113.0	1.292	3.08
3	496	17.62	34.5	38.9	138.0	1.266	3.01
4	506	22.92	35.0	31.1	125.2	1.705	4.06
5	499	20.19	33.4	36.4	140.2	1.413	3.36
6	514	17.70	33.0	45.3	162.8	1.261	3.00
7	517	17.91	31.9	44.9	150.0	1.244	2.96

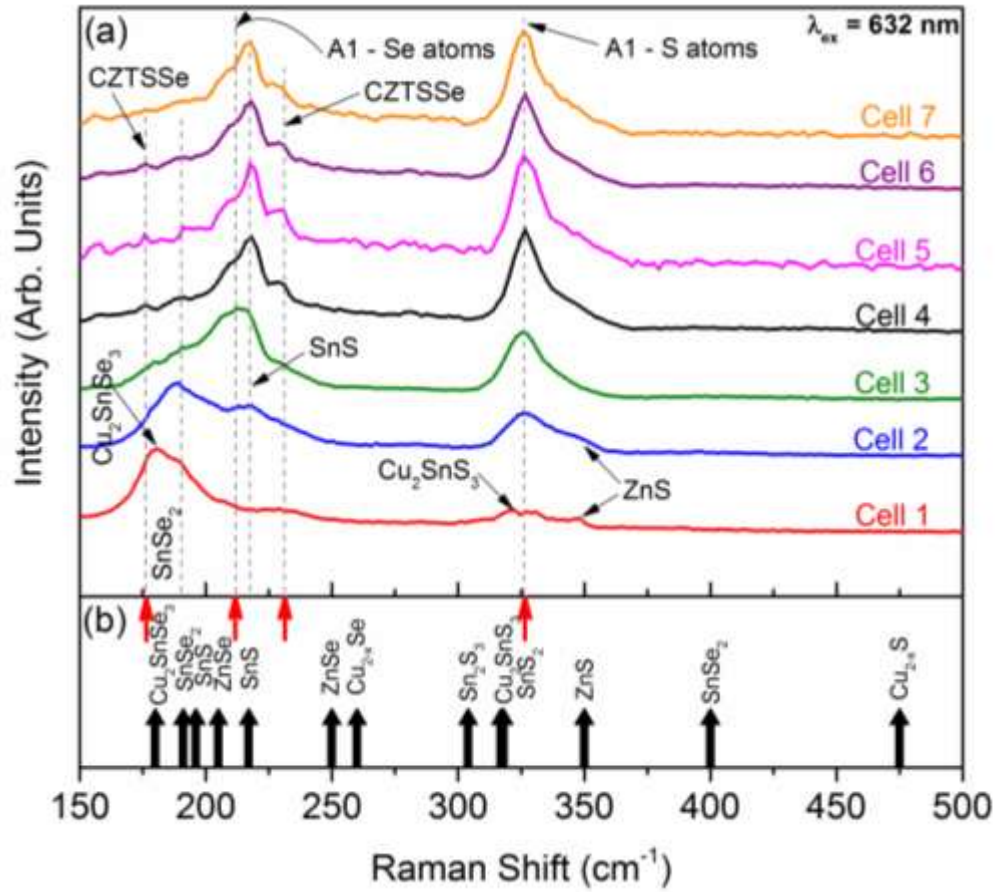


Figure 1. (a) Raman spectra of the CZTSSe film corresponding to the cells obtained using precursor stack 3c, (b) reference Raman peak positions for different possible secondary phases and kesterite CZTSSe phase.

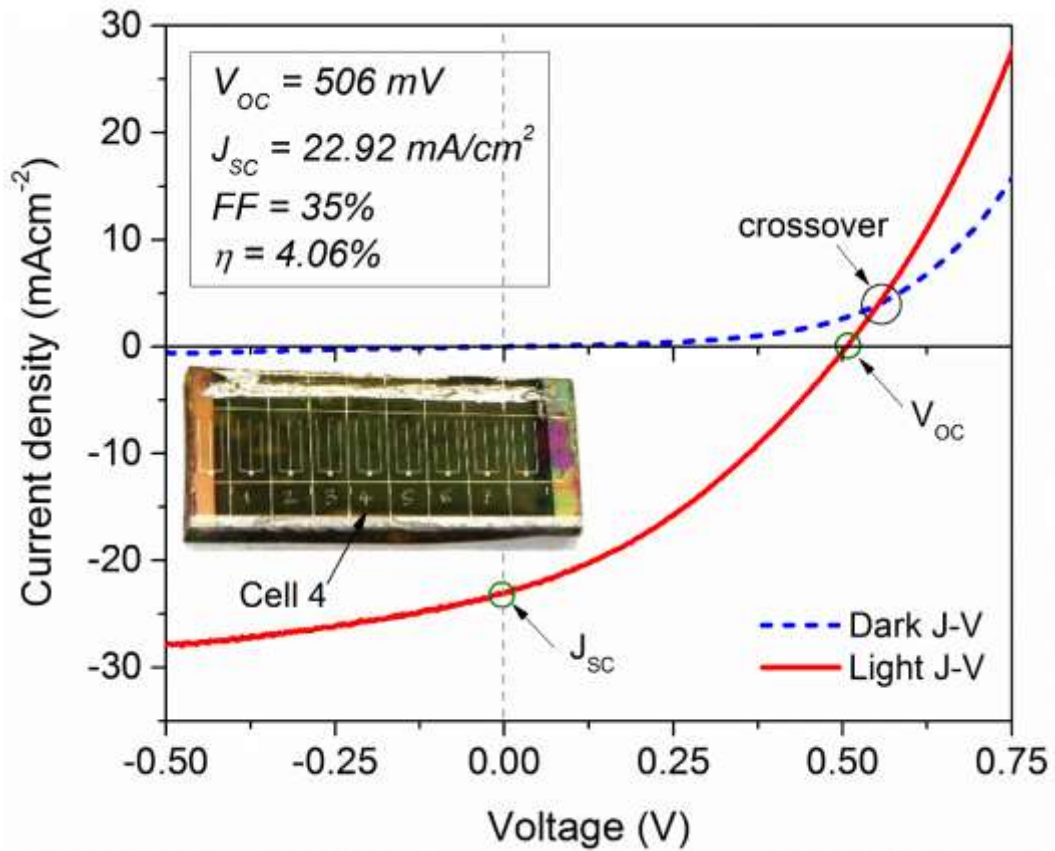


Figure 2. J-V characteristics of the champion cell (cell 4) under dark and under AM 1.5 illumination. [Inset: Photograph of the solar cell array including cell 4].

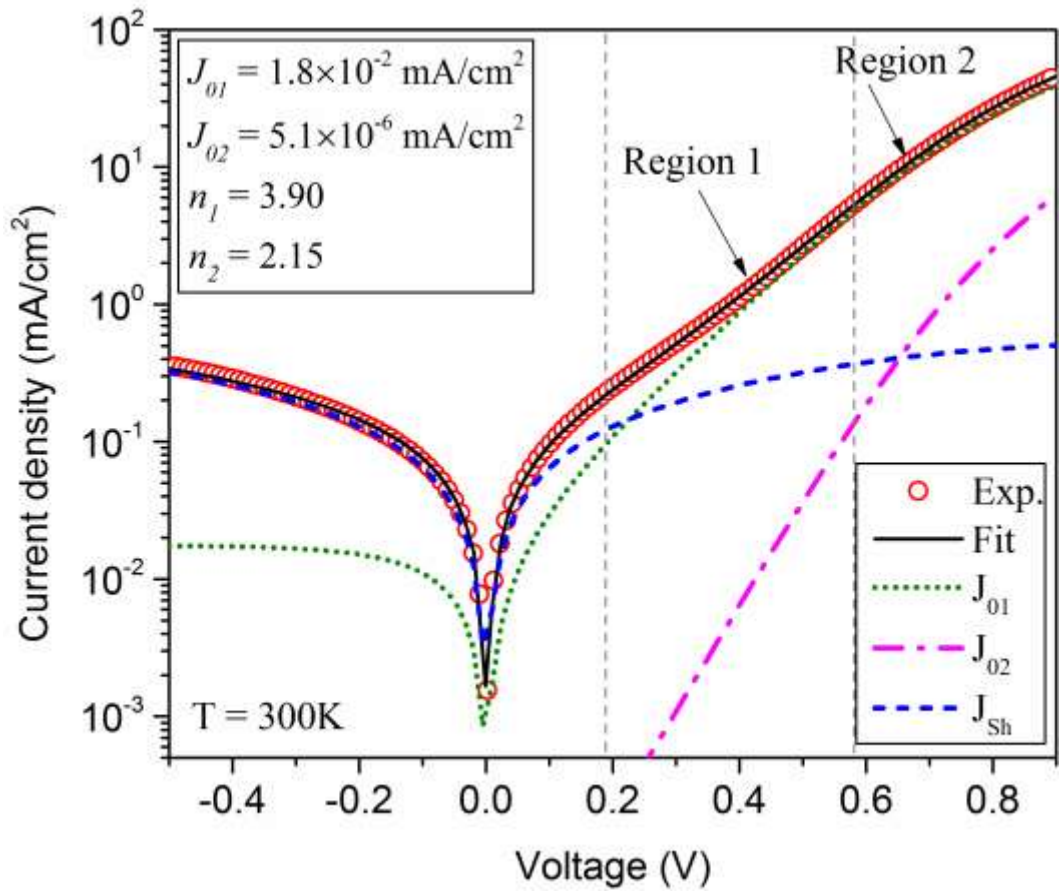


Figure 3. Dark J-V characteristics of cell 4 at 300K and the two-diode model fit.

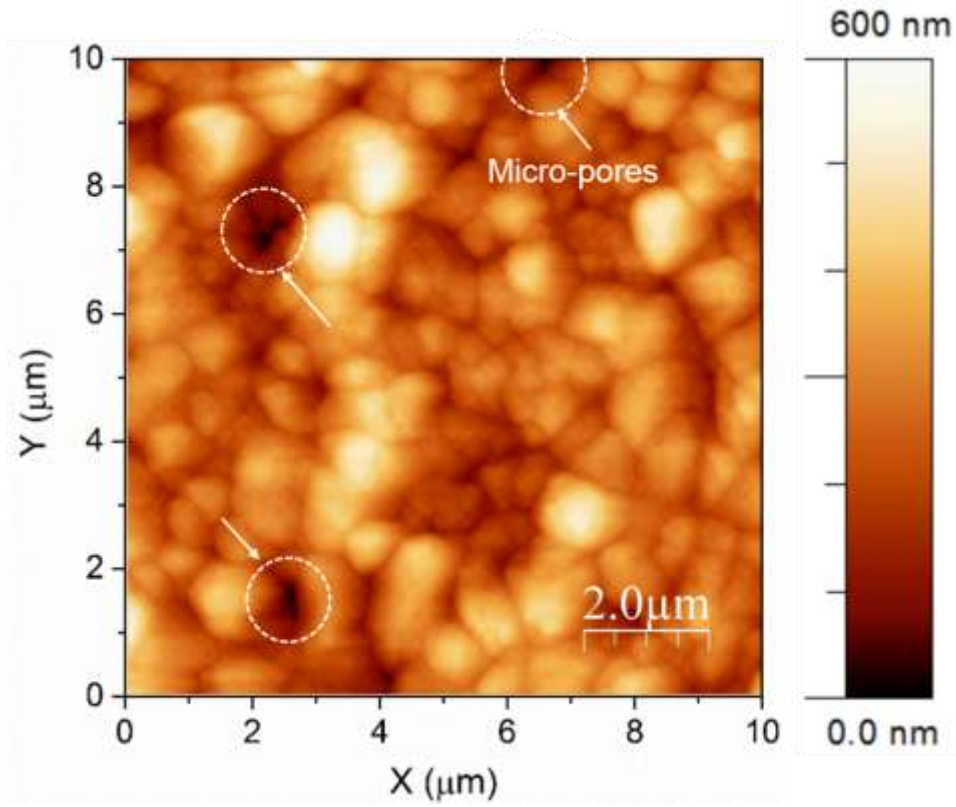


Figure 4. AFM image of the CZTSSe absorber layer surface showing the morphological features.

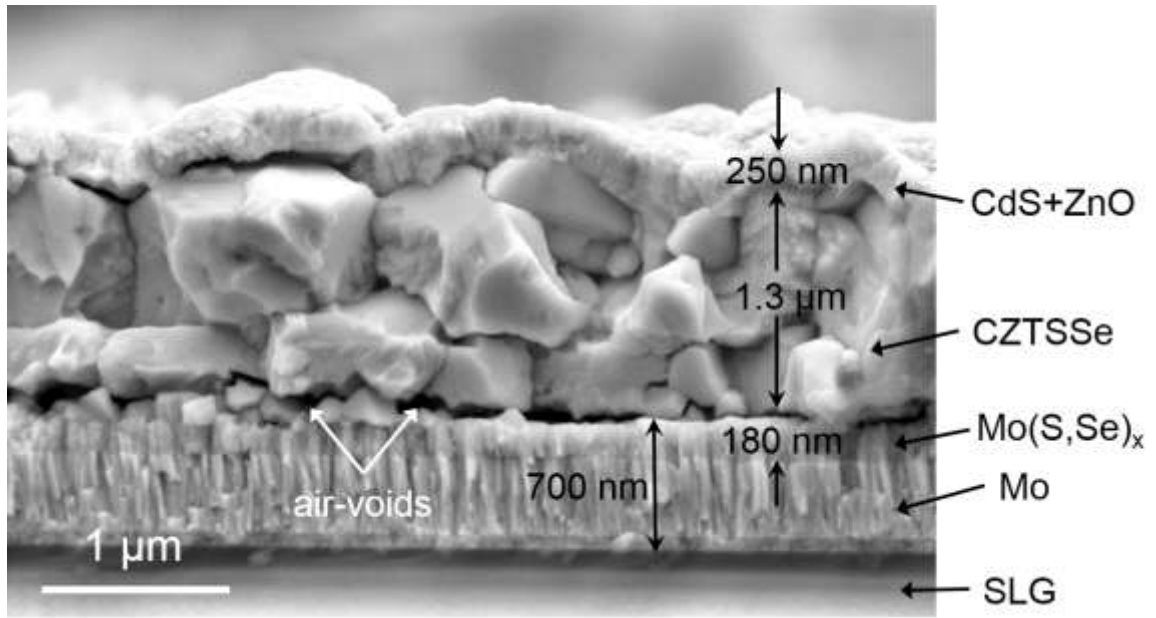


Figure 5. Cross-sectional SEM image of the solar cell.

